Toward biologically meaningful net carbon exchange estimates for tall, dense canopies: multi-level eddy covariance observations and canopy coupling regimes in a mature Douglas-fir forest in Oregon

Christoph K. Thomas[a,b,*], Jonathan G. Martin[b], Beverly E. Law[b], Kent Davis[b]

[a] *College of Earth, Ocean & Atmospheric Sciences, Oregon State University, Corvallis, OR, USA*
[b] *College of Forestry, Oregon State University, Corvallis, OR, USA*

Abstract

We sought to improve net ecosystem exchange (NEE) estimates for a tall, dense, mature Douglas-Fir forest in the Oregon Coast range characterized by weak flows, systematic wind directional shear, and limited turbulent mixing throughout the diurnal period. We used eddy covariance (EC) observations at two levels and concurrent biological measurements of carbon and water fluxes collected over a period of 6 years (2006-2011) to develop and test a conceptual framework to i) reduce uncertainty by retaining more measurements for the computation of annual NEE sums, and ii) produce defendable and biologically meaningful estimates by accounting for the missing sub-canopy respiration. The framework assumes that a) the scalar exchange between vertical layers can be categorized into discrete canopy coupling regimes, and b) advection leads to a systematic loss of scalar from the observational volume

*Corresponding author. Phone: +1 541 737 7690; Fax: +1 541 737 2064; E-mail address: chthomas@coas.oregonstate.edu

that can indirectly be estimated and accounted for as sub-canopy respiration flux when canopy layers are decoupled.

Periods with a decoupled sub-canopy layer dominated and occupied 65 and 88 % of the day- and nighttime periods, respectively. Annual NEE derived from the new framework was estimated as 480 gC m^{-2} yr^{-1}, which was reduced by 620 gC m^{-2} yr^{-1} compared to traditional estimates from single-level EC data filtered using a critical friction velocity. The reduced NEE was due to an enhanced ecosystem respiration (RE), while gross ecosystem productivity remained unchanged. Improved RE estimates agreed well with those from independent estimates based on soil, stem, and foliage respiration within 3 %. Risks and limitations of the new framework are discussed. We conclude that concurrent above- and sub-canopy EC observations are essential to measure a meaningful carbon balance in tall, dense forests since they do no lend themselves to traditional, standardized processing. The new framework may help to include more tall and dense forests in global carbon cycle synthesis and modeling efforts.

Keywords: Net ecosystem exchange, Ecosystem respiration, Advection, Eddy covariance, u-star correction, Canopy flow, Douglas-Fir, Turbulence

1. Introduction

The net ecosystem exchange NEE is the single most important parameter describing the strength of the carbon sink or source of terrestrial ecosystems. Its estimation has received much attention in the literature and a commonly identified obstacle is the 'nighttime problem' when weak turbulent mixing becomes limiting and the computed NEE from a simplified mass balance ap-

proach may not reflect ecosystem functioning (see Goulden et al., 1996; Aubinet et al., 2000; Baldocchi, 2003; Papale et al., 2006, and references therein). The simplified mass balance approach defines NEE as the sum of the turbulent vertical carbon dioxide or methane flux observed above the canopy and the temporal change in storage term from profile observations. In contrast, during the day when mixing is enhanced through stronger flows and significant heat flux, estimates of NEE are typically assumed to reflect ecosystem response to environmental drivers such as light, nutrients, and water independent of the strength of the turbulent transport. Global NEE estimates are modeled based on continental observational networks representing the major biomes, but the selection of individual sites within the networks may be biased toward short vegetation such as grass, open shrubland, and forest. In these canopies, mixing of the scalar sinks and sources can sufficiently well be estimated using variety of mixing indicators. Quantities that have been proposed as a proxy for the turbulent mixing strength include the standard deviation of the vertical velocity variance σ_w (e.g. Acevedo et al., 2009), the friction velocity u_* (e.g. Goulden et al., 1996), their non-dimensional ratio $\sigma_w u_*^{-1}$ termed the integral turbulence characteristic (e.g. Foken and Wichura, 1996; Thomas and Foken, 2002), the mean wind speed U (e.g. Suyker et al., 2003), and a modified turbulent kinetic energy scale u_{TKE} (Wharton et al., 2009). The indicators are typically evaluated from eddy covariance (EC) measurements with a fixed perturbation time scale of 30 or 60 min taken at a single level above the main canopy. However, dense canopies pose additional challenges as they suffer from a night- and daytime problem, since the dense crown space with the maximum plant area index (PAI) presents

a mechanical barrier and efficient momentum sink throughout the diurnal cycle leading to a frequent, persistent decoupling of the sub-canopy from the overstory and above-canopy layers (e.g. Thomas and Foken, 2007; Belcher et al., 2008). In contrast, short vegetation and open forests are only temporally limited by turbulent mixing when surface heating and the mean flow are weak, which typically occurs at night in the absence of significant synoptic meso-scale forcing. As a result, forests with high-PAI, closed canopies are often excluded from network syntheses for reasons of uncertain data quality and insufficient number of observations, since many measurements need to be discarded for the computation of seasonal and annual NEE because of the systematic turbulence limitations. However, these ecosystems may be very efficient carbon sinks as demonstrated by their high PAI, which can only be sustained in high productivity ecosystems. Hence, we identify a significant observational, modeling, and interpretational problem when assessing regional to global carbon balances and their dynamics without the inclusion of tall and dense forests.

In this study we seek to improve NEE estimates for a very dense mature Douglas-fir stand analyzing six years of concurrent EC flux observations at two levels, above the main canopy crown and in the clear bole space below the main canopy crown, with the following objectives:

- identify a simple and meaningful estimator for canopy mixing, coupling, and decoupling that reflects characteristics of the mean flow and the turbulent carbon, sensible and latent heat, and momentum fluxes,

- construct an alternative and practical theoretical framework for the evaluation of multi-level EC observations to estimate NEE,

- increase the fraction of sub-daily NEE estimates that are retained for the computation of seasonal and annual sums, which are assumed to reflect ecosystem behavior,

- compute an improved carbon balance by applying the proposed framework to the observations.

We do not expect this study to solve the problem of overestimating NEE by systematically missing ecosystem respiration, but it may be an important step toward producing defendable and biologically meaningful estimates for dense canopy sites. The ultimate goal is to include these ecologically important sites into network syntheses and global estimates. We further aim at demonstrating the utility of concurrent sub-canopy EC observations to better understand turbulent mixing and other micrometeorological processes in dense canopies. In the literature, only few studies exist that utilize sub-canopy EC observations with the intention of either incorporating their flux estimates into the carbon mass balance or partitioning net carbon fluxes into its components (e.g. Misson et al., 2007; Falk et al., 2008). A number of recent studies has focused on evaluating the advective terms directly using sensor networks and include their flux contributions to the mass balance (e.g. Feigenwinter et al., 2004; Staebler and Fitzjarrald, 2004; Aubinet et al., 2005), while the success of these efforts has recently been questioned (Aubinet et al., 2010).

2. Conceptual framework

Figure 1 placed here.

Diagnosing the dynamics of the canopy flow and its turbulence is critical to connecting the biologically active surfaces such as the foliage, stems, and the soil with the micrometeorological sensors used to quantify the ecosystem scalar exchange. The conceptual framework presented here is based on two major assumptions: first, coupling between vertical layers of the soil-plant-air continuum and thus the exchange of scalar flux varies depending on the strength of the turbulent mixing, which can be diagnosed using multi-level turbulence statistics. Secondly, both vertical and horizontal advection is the main transport mechanism removing the scalar from the observational volume when layers are decoupled. The concept of vertical communication of air across the canopy profile is based on the exchange regimes proposed by Thomas and Foken (2007) for a tall, moderately dense spruce canopy with a PAI of 5.2. Their work differentiates between different conceptual vertical layers which together comprise most of the roughness sub-layer (Fig. 1): i) the above-canopy layer between the top of the overstory and the upper EC observation height, ii) the overstory where most of the PAI is concentrated, iii) the sub-canopy layer or the clear bole space with minimum PAI, and iv) the ground layer including the soil surface and understory including herbs and shrubs often comprising a secondary maximum in the PAI profile. For a typical EC setup located above the canopy at $zh_c^{-1} \approx 1.2$ to 1.8, where z is the observation and h_c the mean canopy height, to measure the entire ecosystem, i.e., integrate over all its vertically distributed scalar sources and

sinks, one must assure that turbulent eddies communicate across all three interfaces between these four layers. In their approach horizontal heterogeneity and transport were originally neglected, but were investigated later by Serafimovich et al. (2011). Thomas and Foken (2007) proposed five exchange regimes with increasing degree of vertical communication between the layers using turbulence measurements at five observation levels to determine the penetration depth and flux contribution of mixing-layer type eddies. They demonstrated that the sub-canopy layer is often decoupled from the crown and free roughness sub-layers even during the day when the above-canopy flow and turbulent mixing are significant. A recent study by Foken et al. (2012) confirmed the utility of this concept when investigating the dynamics of ecosystem fluxes of volatile organic compounds, nitrous oxides, and ozone. The authors concluded that the observed concentration profiles and fluxes could only be explained when the cross-interface transport was diagnosed using the exchange regimes, while other simpler methods including the critical u_* threshold approach (Goulden et al., 1996) failed.

Since extensive multi-level EC observations and complex post-processing are impractical and probably cost-prohibitive for long-term ecosystem studies targeting measuring NEE on annual and decadal time scales, we simplified the method. The method proposed here diagnoses the cross-interface transport based on only two observational heights located in the above- and sub-canopy layers while retaining the concept of exchange regimes and layers. We further added a concept originally proposed by Scanlon and Albertson (2001) to use scalar-scalar cross-correlations between perturbations in carbon dioxide and water vapor mixing ratios to partition scalar sinks and sources.

Instead of partitioning, we here invert the original idea and apply it to diagnose the communication of air across the canopy profile by relating the scalar-scalar fingerprint to the turbulent mixing strength. The simplified conceptual framework differentiates between three exchange regimes:

- Fully coupled canopy (C): Above-canopy EC fluxes fully integrate over all scalar sinks and sources and are representative of the entire ecosystem. This is the ideal state typically assumed for traditional EC analysis of NEE.
- Decoupled sub-canopy (Ds): Fluxes observed with the sub-canopy EC system integrate the scalar sinks and sources of the ground and sub-canopy layers, but are decoupled from those of the overstory and above-canopy layers.
- Decoupled ground layer (Dg): Fluxes observed with the sub-canopy EC system are not coupled to the soil and ground vegetation, i.e., do not represent soil CO_2 efflux, photosynthesis and autotrophic respiration of the ground layer. This regime was originally not included in the concept by Thomas and Foken (2007) since transport across the soil-air interface was neglected.

Table 1 placed here.

We emphasize that the biological processes of respiration and assimilation are continuous in time. However, when ground and sub-canopy layers are decoupled (Dg, Ds regimes), their signals and flux contributions are not

properly captured by the micrometeorological instrumentation and simplified mass balance approach due to limited turbulent transport and mixing. As in most NEE studies, the simplified mass balance approach deployed here does not directly measure the advective transport and neglects the pressure transport and the horizontal flux divergence terms. For a fully coupled canopy (C), advection is assumed to be negligible and the ecosystem-scale net ecosystem exchange is the defined as the sum of vertical turbulent flux and temporal change in storage term, i.e.,

$$NEE = FCO_{2,top} + \Delta S. \tag{1}$$

The terms are defined as

$$FCO_2 = \rho\overline{w\prime\chi_c\prime}\ ,\ \Delta S = \int \left(\frac{d\chi_c}{dt}\right) dz, \tag{2}$$

with the subscript 'top' denoting the above-canopy EC level, w is the vertical wind component, χ_c the mixing ratio of carbon dioxide, ρ air density, and the overbar represents the temporal average and the prime the perturbation thereof. However, when decoupling limits the vertical exchange across the interface between the sub-canopy and canopy layers (Ds regime), we assume that advection becomes important and can indirectly be estimated and accounted for by adding the sub-canopy respiration flux Re_{sub} to the simplified carbon mass balance, which leads to

$$NEE = FCO_{2,top} + Adv + \Delta S \approx FCO_{2,top} + Re_{sub} + \Delta S. \tag{3}$$

170 Adv is the sum of vertical and horizontal advection, and the subscript 'sub'
171 denotes the sub-canopy EC level. The validity of this assumption will be dis-
172 cussed in Section 4.6. Re_{sub} was quantified following the method of Thomas
173 et al. (2008), which applies a relaxed eddy accumulation approach to the
174 sub-canopy EC observations to sample episodic respiration pulses used to
175 construct flux estimates. A brief overview of this method is given in Section
176 3.2. Note that $\mathrm{Re}_{sub} \neq \mathrm{FCO}_{2,sub}$, the latter being the net carbon exchange
177 observed by the sub-canopy EC system. Although this approach was origi-
178 nally proposed for daytime conditions only, the method is equally applicable
179 to nighttime conditions due to the persistence of the scalar-scalar correla-
180 tions between carbon dioxide and water vapor in the sub-canopy.
181 In traditional single-level EC NEE studies only data for a fully coupled
182 canopy (C), typically diagnosed by exceeding a critical threshold of the fric-
183 tion velocity, can be used to compute a biologically meaningful NEE. In con-
184 trast, the improved method proposed here allows for computation of NEE
185 also when the turbulent exchange of air between the sub-canopy and the
186 crown is significantly inhibited (C + Ds). Both methods fail to produce a
187 meaningful NEE for conditions when the sub-canopy is decoupled from the
188 ground layer (Dg). A summary of the applied mass balances to compute
189 the improved NEE estimates depending on the light and canopy exchange
190 regimes is given in Table 1. Note that for our site the photosynthetic uptake
191 of the understory GEP_{sub} was neglected for NEE computations because of the
192 very low photosynthetic photon flux densities measured in the sub-canopy
193 that reach maximum values of < 50 μmol m^{-2} s^{-1} during summer months
194 (Thomas, 2011).

3. Methods & Materials

3.1. Measuring the turbulent fluxes and change in storage term

The turbulent fluxes of momentum τ and its related generalized friction velocity $u_* = \sqrt{\frac{\tau}{\rho}} = \sqrt[4]{\overline{u\prime w\prime}^2 + \overline{v\prime w\prime}^2}$, carbon dioxide FCO_2, and water vapor $\lambda E = \rho\overline{w\prime q\prime}$ were computed as covariances from high-frequency measurements sampled at 20 Hz. The symbols u, v, w stand for the along, cross, and vertical wind velocities respectively, and q is the water vapor mixing ratio. Wind vector components were transformed prior to computing fluxes and flow statistics using a double-rotation matrix consisting of median rotation angles computed for wind direction sectors that contain an equal number of data over one year. The philosophy behind this rotation is similar to that of the planar-fit rotation method (Wilczak et al., 2001), but the streamlines are not forced through a plane and the statistical uncertainty of the rotation angles across all wind direction sectors is identical. At our site, the mean streamlines do not fall on to a plane because of the mountainous terrain. The perturbation time scale to compute excursions from mean quantities for the above-canopy system was chosen as 30 min, while 6 min were used for the sub-canopy observations based on co-spectral analysis to minimize the influence of motions other than turbulence introducing non-stationarities. It also enables one to relate the turbulent fluxes and flow statistics to properties of the generally weak sub-canopy mean flow (see Section 3.4). Subsequently, five 6-min sub-canopy fluxes were averaged into one 30-min estimate to minimize the random error and to match the temporal resolution between both EC systems. The upper EC system was located above the canopy at 37.4 m above ground level (agl), i.e., at $zh_c^{-1} = 1.4$, and consisted of a sonic

anemometer (Model CSAT3, Campbell Sci., Logan, UT, USA) in combination with open- (Model Li-7500, Licor Env., Lincoln, NE, USA) and closed-path (Model Li-7000, Licor Env., Lincoln, NE, USA) infra-red gas analyzers recorded by a data logger (Model CR5000, Campbell Sci., Logan, UT, USA). From Jan 2007 until Dec 2008, both infra-red gas analyzers were run in parallel continuously for cross-validation of carbon dioxide and water vapor fluxes showing only small deviations from a 1:1 relationship. Starting Jan 2009, the closed-path gas analyzer was chosen to be the primary instrument for flux measurements because of the frequent and abundant winter precipitation, while the open-path analyzer was brought online for episodic comparison during the drier summer each year. The closed-path analyzer was housed in a custom-designed, insulated, and temperature-controlled aluminum case at the top of the tower. The sample gas was drawn via an electric brushless pump (Model 6025SE, Thomas, Sheboygan, WI, USA) through a 7 m-long insulated, heated, and pressure regulated (Model 640, MKS Instr., Andover, MA, USA) stainless steel line of 6.35 mm (1/4 in) outer diameter equipped with two 1 μm Gelman filters yielding a mean flow of 5 to 8 l min^{-1} depending on pump supply voltage. The flow rate was monitored, recorded, and in combination with the analyzer status flag used to quality-filter the data. The lower, sub-canopy system was located at 4 m agl, i.e., at $zh_c^{-1} = 0.14$, and consisted of a sonic anemometer in combination with an open-path analyzer recorded by a data logger identical to those used for the upper EC system. Fluxes computed from open-path analyzer measurements were subject to a post-hoc density correction (Webb et al., 1980). Aspirated air temperature T, relative humidity rH, net radiation R_{net}, and barometric pressure p, were

continuously measured at both observations levels, while short- and longwave radiation components and the photosynthetic photon flux density (Models CNR-1 and PARlite, Kipp&Zonen, Delft, The Netherlands) were observed only above the canopy at the tower top.

The change in storage term ΔS (see Eq. 2) was estimated by measuring the temporal dynamics of the carbon dioxide mixing ratio across a vertical profile sampled at 7 heights at 0.5, 1.7, 4.0, 9.0, 18.0, 27.0, 37.9 m agl several times within a 30-min period using an infra-red gas analyzer (Model Li-820, Licor Env., Lincoln, NE, USA) operating at 1 Hz. This custom-made CO_2 profile system followed the design by Stephens et al. (2006) with major modifications to minimize fluctuations in pressure, air temperature, and water vapor (Gockede et al., 2010). Calibration and quality control of the raw data was based on four NOAA-ESRL gas standards sampled at regular intervals.

3.2. Computing the sub-canopy respiration flux

When the above- and sub-canopy layers are decoupled (Ds), the sub-canopy respiration flux is an important quantity in the carbon mass balance accounting for the advective loss (see Eq. 3 and Table 1). Re_{sub} was computed using the modified relaxed eddy accumulation method of Thomas et al. (2008) applied to the sub-canopy EC observations. The sub-canopy respiration includes the contributions of the root, litter, and microbial respiration and respiratory signals of the coarse and fine woody detritus and understory vegetation. For each 6-min interval, the method identifies individual data points in the continuous EC time series that represent excursions from similarity-theory predictions of the correlation structure between perturbations of carbon dioxide and water vapor mixing ratios that are associated

with updrafts. These excursions can then collectively be used to construct a flux estimate. The underlying assumption is that updrafts ($w\prime > 0$) carrying the sub-canopy respiration signal have a different, positively correlated scalar-scalar fingerprint with $\chi_c\prime > 0$ and $q\prime > 0$. In contrast, motions carrying the fingerprint of the canopy crown show a negative correlation between $\chi_c\prime$ and $q\prime$. To include only those excursions into the computation of Re_{sub} that carry a strong sub-canopy respiration signal, a hyperbolic hole of the size H_{Re}=0.5 is applied to the correlation diagram constructed from plotting $\chi_c\prime$ versus $q\prime$. The excluded data falling into the area of H_{Re} <0.5 may contaminate the resulting sub-canopy respiration fluxes. Thomas et al. (2008) found a hole size of H_{Re} =0.25 to be adequate using data from a range of different sites including the one investigated here for both above- and sub-canopy EC observations. A comparison of different hole sizes for our data yielded that Re_{sub} was only slightly sensitive to the choice of H_{Re}. Re_{sub} estimates for individual 6-min periods were only accepted and processed further when the fraction of excursions from similarity theory predictions exceeded 8 % of the total data (τ_{Re}, for details see Fig. 7 in Thomas et al., 2008). This criterion corresponds to $r_{c,q} \geq 0.1$ for the threshold of the transition from the decoupled ground layer (Dg) to decoupled sub-canopy (Ds) regimes discussed later (see Fig. 5a). As mentioned in the previous section, flux estimates from a maximum of 5 subsequent 6-min periods were then combined into one 30-min average. If none of the 6-min periods within a 30-min interval fulfilled this condition, NEE could not be computed from observations according to Eq. 3, but was modeled. One must note that $\mathrm{Re}_{sub} \neq \mathrm{FCO}_{2,sub}$ for the decoupled exchange regime since the turbulent eddies transporting the CO_2 molecules

released by the biologically active surfaces into the sub-canopy air do not exchange with the layers aloft, but transport the scalar passively in up- and downdrafts with their stochastic motion (see center panel of Fig. 4 in Zeeman et al., 2012). As a result, the sub-canopy net carbon dioxide flux $FCO_{2,sub}$ underestimates the sub-canopy respiration flux assumed to be advected.

3.3. Computing alternative ecosystem respiration

In order to verify the ecosystem respiration estimates computed from the new framework, they were compared against a completely independent estimate (see Sections 4.4 and 4.5). This alternative estimate of ecosystem respiration RE_{alt} was constructed from chamber-based respiration measurements and models of foliage and stem tissues, as well as total soil respiration. Foliage respiration Re_{fol} was measured on a 8 branches from four individual trees from mid to upper canopy positions at the end of summer (DOY 243, 2011) using a portable photosynthesis system (Model LiCor 6400, Licor Env., Lincoln, NE, USA). Branches were cut prior to sunrise, cut ends were placed in water and returned to the lab where measurements were made at a standard temperature (25 °C) between 06:00 and 09:00 local time. Foliage samples were dried at 40 °C and analyzed for carbon and nitrogen concentrations (Model LECO CNS 2000 analyzer, Leco Corp., St. Joseph, MI, USA). The resultant respiration values were standardized to 20 °C and compared to published values from meta-analysis work where reference values of mass based respiration (R20, respiration values at 20 °C) were a function of nitrogen (N) concentration (Reich et al., 2008). Our foliar respiration per unit N values were slightly lower and required a correction factor of 1.13. Additionally, a seasonal time course of N was used to scale the R20 values

for temporal N allocation patterns (Matson et al., 1994). The seasonally dynamic R20 was then combined with the acclimation response of Q10 to temperature history (Atkin and Tjoelker, 2003; Tjoelker et al., 2001). The combined model was driven by sub-canopy air temperature while the base rate was modulated by seasonal N and the Q10 was dynamic in response to the 4 day running mean of sub-canopy air temperature. These mass-based estimates of foliage respiration were then scaled to ground area using a leaf mass per area of 78.12 gC m^{-2} and a site level PAI of 9.4 m^2 m^{-2}. Stem respiration Re_{st} on a sapwood volume basis and concurrent stem temperature at 0.05 m depth was measured on 8 trees (see methodology in Law et al., 1999) over multiple temperature conditions with 3 trees monitored continuously for detailed temperature responses over different 3 day periods to provide a large temperature range (temperature range of 11 to 19 °C). The averaged temperature responses were adjusted using the mean values from the remaining trees. This temperature response was then applied to continuous records of soil temperature at 0.08 m depth, which closely matched point measurements of stem temperature, and scaled to the site using year specific estimates of sapwood volume. Soil respiration Re_{soil} was measured every 4 hours continuously on six chambers (methodology and system construction can be found in Irvine and Law, 2002). Hours between measurements were linearly interpolated while gaps larger than 2 measurement cycles were filled using a temperature and soil moisture model which performed well at this site and adequately captured the variation and timing of diurnal trends (Martin et al., 2012). Temporal coverage of available 4 hour periods was > 65 %. All modeling and gap filling was performed on individual chambers; these

records where then averaged and scaled to the site using extensive spatial data from 3 to 5 periodic spatial surveys per year on 20 separate locations (see details in Thomas et al., 2009; Vickers et al., 2012). Soil temperature was recorded hourly using 3 arrays of thermocouples at 0.02, 0.04, 0.08, 0.16, 0.32 and 0.64 m depth. Soil volumetric water content was measured using probes integrating over the upper 0.3 m (Model CS615, Campbell Sci., Logan, UT, USA).

3.4. Architecture and mean flow characteristics of the research site

Figure 2 placed here.

The dataset was collected in a 36 year-old mature Douglas-Fir (*Pseudotsuga menziesii, Mirb.)* forest located in the coast range of western Oregon, USA (AmeriFlux site US-Fir, 44.646° N latitude, 123.551° W longitude, 310 m elevation) surrounded by mountainous terrain with a flat saddle located to the northeast of the tower at a distance of approximately 600 m (see Figure 1 in Thomas, 2011). Observations described in this study were collected between May 01, 2006 and Nov 03, 2011, i.e., over a period of approximately 5.5 years. The vertical structure of the vegetation canopy with a mean height $h_c = 28$ m consists of a sparse understory composed mainly of Salal (*Gaultheria shallon, Pursh*) with a plant height of up to 0.8 m agl and the main tree crown space extending from 15 to 28 m agl separated by a clear bole space. The canopy is very dense with a plant area index (PAI) of 9.4 $m^2\ m^{-2}$ optically measured in 2004 (Model LAI2000, Licor Env., Lincoln, NE, USA).

The vertical structure of the canopy and the high PAI lead to generally very weak flows in the sub-canopy characterized by a median horizontal wind speed $U \approx 0.5$ m s^{-1} and a 98 %-percentile of 1 m s^{-1} irrespective of light

regime (Fig. 2b). In contrast, above-canopy wind speeds are significantly stronger with a median of 1.6 and 1.2 m s^{-1} during day and night respectively (Fig. 2a). In comparison with other sites, both above- and sub-canopy speeds are generally weak because of the orographic sheltering provided by the surrounding ridges. All wind speed distributions have a positive skewness indicating a preference for weaker winds. Above the canopy, the distribution of wind directions is strongly bimodal with preferred flows from west-south-west (250°) and east (90°), which is representative of the regional flow. At night, easterly drainages are relatively more common compared to daytime at the expense of westerly flows (Fig. 2c). The comparison of wind directions between both levels indicates a systematic wind directional shear at the site. For above-canopy flows centered around south-west and north-east the wind directional shear reaches a maximum of 150° indicating almost opposite flow directions. The existence of wind directional shear is insensitive to the light regime, but its north-east maximum broadens at night to span a sector between north-west and north-east. Although these wind directions are less common and the wind directional shear for the two main wind sectors is typically $\Delta\phi \leq 40°$, the directional shear in conjunction with significant stratification generated additional mixing and impacted the classification into exchange regimes as discussed in Section 4.2.

Previous studies investigating processes and mechanisms contributing to vertical coupling and decoupling at this sites yielded two main results: Thomas et al. (2008) reported that the attempt to estimate the sub-canopy daytime respiration from above-canopy EC measurements failed as the dense overstory acts as a mechanical barrier, which leads to a loss of the carbon dioxide

- water vapor fingerprint of air originating in the sub-canopy and ground layers. A follow-up study by Zeeman et al. (2012) found that larger-scale motions including mixing-layer type coherent structures and convective plumes are not the main flow mode responsible for transporting scalars through the dense overstory, but concluded that small-scale stochastic turbulence was the main transport path. The authors confirmed that the scalar-scalar cross-correlations observed above the canopy showed a weak dependence on ground scalar sources and sinks. In comparison with other sites, both studies demonstrated that the method to partition the sub-canopy respiration flux from NEE measurements succeeded in more open, sparse canopies, as their architecture allows larger motions to penetrate deeply into the canopy forcing the exchange with the sub-canopy and ground layers.

4. Results & Discussion

4.1. Comparing possible mixing indicators

Figure 3 placed here.

In order to assess the strength of the turbulent mixing that serves as an estimator for the degree of coupling across the canopy profile, one needs to find a suitable proxy. We here focus on quantities that are commonly evaluated during EC post-processing. The comparison of friction velocity and the standard deviation of the vertical velocity variance between the above- and sub-canopy levels yielded similarities, but also important differences (Fig. 3a, c): At night when winds are weak, the turbulence strength in the sub-canopy is largely independent of that above the canopy showing an asymptotic behavior toward a constant value, but scales almost linearly after the above-canopy

flow crossed the threshold of $u_* = 0.25$ m s^{-1} and σ_w 0.45 m s^{-1} respectively. During the day when winds are stronger, the behavior is similar, but the thresholds for the transition from the asymptotic to the linear response are smaller at 0.12 and 0.20 m s^{-1} respectively. The scatter on both abscissa and ordinate is significant, particularly for the asymptotic, independent regime. The independence of the sub-canopy turbulence strength from that aloft indicates either different, independently acting mechanisms generating or destroying turbulence, or that the above- and sub-canopy flows are largely decoupled, or a combination of both. In case of the former, the above-canopy flow and its wind speed shear at the canopy top are not the main source of turbulence in the sub-canopy as the penetration of eddies deep into the trunk space is limited by the dense overstory. This interpretation is in agreement with the findings of Zeeman et al. (2012) who investigated the penetration depth of larger-scale including mixing-layer type structures and convective plumes at the same site. If the above- and sub-canopy flows are decoupled, the existence and passage of sub-meso motions on scales larger than those of turbulence could be responsible for the generation of sub-canopy turbulence (Thomas, 2011). Sub-meso motions are always present in the atmosphere, but tend to dominate dispersion and turbulent diffusion only when the mean flow is very weak (Mahrt et al., 2009), such as in canopy flows. Note that for a given turbulence strength above the canopy, the sub-canopy equivalent is larger at night than during the day. An explanation for this observation is the temporally reversed stability regime between the above- and sub-canopy layers typical for dense forests: during the day when the radiative heating of the overstory leads to free convection and a maximum temperature lo-

cated near the PAI maximum, the sub-canopy is slightly stably stratified acting to suppress turbulence; at night when progressive radiative cooling of the crown leads to increasing static stability in the above-canopy layer, the sub-canopy layer becomes isothermal or slightly unstable acting to enhance turbulence. One feature worth noting is the increase of sub-canopy turbulence strength for very weak above-canopy turbulence, which was associated with the generation of additional mixing by wind directional shear, which will be discussed in the next section. Wind speeds in the above- and sub-canopy layers are related by a weakly non-linear relationship depending on the light regime (Fig. 3b). As for the turbulence, the nighttime sub-canopy flow tends to be stronger for a given above-canopy wind speed exceeding $\geq$ 1.5 m s^{-1} than during the daylight hours. During the day, both above-canopy u_* and σ_w respond non-linearly to an increase in wind speed up until $\approx$ 1.5 m s^{-1}, after which the relationship becomes strictly linear (Fig. 3d). The initial maximum observed around 1 m s^{-1} can be explained by the generation of turbulence through buoyancy resulting from the radiative heating of the crown, which is important when flows are weak. The linear response for stronger flows indicates the shear-driven turbulence. For the subcanopy, the dependence of the turbulence strength on the mean sub-canopy flow was much weaker (not shown here), accentuating the importance of generating mechanisms for turbulence other than the commonly discussed wind speed shear. At night, both u_* and σ_w scale linearly with wind speed and approach a constant minimum value for $U \rightarrow 0$ m s^{-1}. The identical behavior was observed by Mahrt et al. (2012) for calm near-surface flows above short grass during stable conditions at three different sites in structured, mountainous

terrain. Both ratios $\sigma_w u_*^{-1}$ and $\sigma_w U^{-1}$ showed a maximum for very weak flows while asymptotically approaching a constant value for stronger flows (Fig. 3d).

For the purpose of this study which aims at improving NEE estimates through determining meaningful exchange regimes based on multi-level flow statistics, the most suitable proxies are either the friction velocity or the standard deviation of the vertical velocity variance. Both quantities showed an obvious transition between regimes that may be linked to vertical coupling and decoupling processes as discussed below. We prefer the vertical velocity variance σ_w as the primary indicator of mixing in this study for the following reasons: i) it relates the turbulence strength directly to properties of the mean turbulent flow and not to its turbulent momentum transport as in the case of u_*; ultimately, the turbulent eddies and their associated vertical velocity perturbations lead to diffusion and mixing, and not the momentum transport; ii) it appears to be more sensitive to alternative generating mechanisms for turbulence including sub-meso motions and wind directional shear, which are important in dense canopies; and iii) both day- and nighttime values converge on to the same linear relationship and show less scatter for stronger mixing facilitating the selection of universal thresholds presented in the next section. Our findings are in agreement with Acevedo et al. (2009) who also preferred σ_w over u_* as the mixing indicator to filter nighttime CO_2 fluxes for several forest sites in Brazil. With their choice of σ_w, thresholds for limiting vertical mixing were easier to identify and nighttime NEE estimates were increased in magnitude.

493 *4.2. Enhancing mixing through wind directional shear*

494 Figure 4 placed here.

495 The systematic, substantial directional shear found in the wind climatology
496 (Fig. 2d) led to an increase in mixing strength at night when combined with
497 significant above-canopy flows (see Fig. 4a). For weaker flows, the enhanced
498 mixing generated by the wind directional shear is expected to lead to conver-
499 gence of both flows resulting in $|\Delta\phi_{top-sub}| \rightarrow 0°$. Since wind speed shear, i.e.,
500 the vertical differences of horizontal wind speeds across the canopy profile,
501 is commonly thought of as the main mechanism inducing flow instabilities
502 and creating overturning eddies to generate turbulence at night, the wind
503 directional shear is typically not included in the dynamic stability analysis
504 for canopy flows (e.g. Paw U et al., 1992; Raupach et al., 1996). However,
505 the gradient Richardson number, defined as the ratio of buoyancy to shear
506 terms in the turbulent kinetic energy equation (e.g. Stull, 2000)

$$Ri_{gr} = \frac{g}{\theta_v}\Delta\theta_v\Delta z(\Delta X^2 + \Delta Y^2)^{-1}, \tag{4}$$

507 theoretically includes the effect of directional shear through the differences
508 in zonal ΔX and meridional ΔY wind components; g is the gravitational
509 acceleration on earth and θ_v the potential virtual air temperature. Evalu-
510 ating Ri_{gr} yielded that the sub-canopy mixing strength $\sigma_{w,sub}$ was enhanced
511 only for $U_{top} \geq 1$ m s^{-1} in combination with strong stability $Ri_{gr} > 1$ and
512 $|\Delta\phi_{top-sub}| > 70°$ (Fig. 4b). This enhancement was 50 to 80 % compared
513 to periods when either $|\Delta\phi_{top-sub}| < 50°$ or $0.2 \leq Ri_{gr} \leq 4$ (Fig. 4b, Eq.
514 4). This additional mixing impacted the found exchange regime and thus
515 the computation of NEE. For moderately strong winds $2 < U_{top} \leq 3$ m s^{-1}

the additional mixing led to a fully mixed canopy, albeit the strong stability $Ri_{gr} > 10$ (Fig. 4b). This observation is, however, counter-intuitive given the definition of Ri_{gr} and requires some discussion. Since the directional shear contributes to the denominator in Eq. 4, one would expect Ri_{gr} to decrease with increasing $|\Delta\phi|$. Since the opposite behavior is observed, we conclude that the gradient Richardson number insufficiently reflects the additional mixing induced by the wind directional shear. In contrast, Burns et al. (2011) evaluated flow and scalar statistics in a moderately dense coniferous forest in mountainous terrain and found that binning by the Richardson number was useful to explain vertical scalar mixing. However, the authors used the bulk formulation of the Richardson number Ri_b that is sensitive to wind speed shear only. At their site, the mean wind directional shear vanished for $Ri_b > 0.1$, while its variance increased significantly possibly indicating meandering of the flow.

Note that in our study the presence of wind directional shear between above- and sub-canopy flows is not synonymous with vertical decoupling. On the contrary, it leads to enhanced mixing and a fully coupled canopy under conditions of significant stratification. Note that while mixing is enhanced, it is still weak compared to unstable conditions.

4.3. Defining mixing thresholds for the exchange regimes

Figure 5 placed here.

After identifying a suitable proxy for the turbulent mixing strength, the next step is to connect its behavior to the signals of the biological carbon sinks and sources. The goal is to define biologically meaningful thresholds for the exchange regimes proposed earlier. To that end, we use the same concept

applied earlier when quantifying the sub-canopy respiration flux (see Section 3.2) to distinguish between turbulent eddies that carry the fingerprint of the ground layer from that of the canopy layer. One recalls that following this concept, eddies carrying the fingerprint of the ground layer are expected to show a positive correlation between $\chi_c\prime$ and $q\prime$. In contrast, eddies carrying the fingerprint of the overstory are expected to show a negative correlation between $\chi_c\prime$ and $q\prime$.

The correlation coefficient between perturbations of carbon dioxide and water vapor perturbations $r_{c,q}$ evaluated from the sub-canopy EC data showed a distinct behavior with the turbulent mixing strength irrespective of light regime and seasonality (Fig. 5a): for very weak mixing $\sigma_{w,sub} \leq 0.03$ m s^{-1} the correlation is close to zero and erratic with frequent changes in sign. For $0.03< \sigma_{w,sub} \leq 0.10$ m s^{-1} the correlation becomes systematically positive with $r_{c,q} \geq 0.1$ and increases with increasing mixing strength. If the mixing strength increases beyond $\sigma_{w,sub} \geq 0.10$ m s^{-1}, the correlation systematically declines again and ultimately becomes negative for $\sigma_{w,sub} > 0.2$ m s^{-1}. We here define the first threshold at $\sigma_{w,sub}= 0.03$ m s^{-1} as the transition from the decoupled ground layer (Dg) to the decoupled sub-canopy layer (Ds) regime. Beyond this threshold the sub-canopy EC observations clearly capture the scalar-scalar fingerprint of the sources in the ground layer. Note that the magnitude of the correlation is sensitive to sub-canopy air temperature as the magnitude of the sub-canopy fluxes of respiration and evapotranspiration is seasonally dependent. Strongest correlations were found for the greatest temperatures when fluxes are maximum. The second transition at $\sigma_{w,sub}=$ 0.10 m s^{-1} reflects the transition from the decoupled sub-canopy (Ds) to

the fully coupled canopy (C) regime. As eddies start to communicate across the entire canopy profile, the growing influence of the scalar-scalar fingerprint of the overstory with $r_{c,q}$ <0 leads to a progressive decorrelation of the ground layer fingerprint with $r_{c,q}$ >0. Note that correlating $r_{c,q}$ to the sub-canopy friction velocity showed the same overall behavior (not shown here), but yielded different transitions at $u_{*,sub}$= 0.02 m s^{-1} from Dg to Ds, and at $u_{*,sub}$= 0.10 m s^{-1} from Ds to C (Table 1). Our interpretation of the connection between increasing sub-canopy mixing strength and enhanced mass transport exchanging scalars across the entire canopy is different from that based on analyzing the momentum exchange in tall, but low PAI forests (e.g. Shaw and Zhang, 1992; Dupont et al., 2012). Based on observations and large eddy simulations in stands with PAI $\leq$ 2.5, these studies concluded that much of the sub-canopy turbulence is generated by pressure transport from aloft. While pressure diffusion may be an important mechanism generating mixing in the sub-canopy, these studies did not directly evaluate the air and scalar exchange which may follow perturbations in the pressure field. Flow visualizations using machine-generated fog at our site confirmed our interpretation of mass exchange between the ground, sub-canopy, overstory, and above-canopy layers that is associated with significant sub-canopy mixing. The validity of our interpretation to define meaningful exchange regimes based on $\sigma_{w,sub}$ is further discussed in Section 4.6.

For above-canopy observations, the concept of $r_{c,q}$ changing sign is not applicable since carbon dioxide and water vapor perturbations are systematically negatively correlated. We here use the traditional nighttime plot of (FCO$_{2,top}$ + ΔS) versus turbulent mixing strength to define a threshold for coupling be-

tween the above-canopy EC system and the tree crown. At night, ($FCO_{2,top}$ + ΔS) becomes independent of turbulent mixing strength for $\sigma_{w,top} \geq 0.45\,\mathrm{m\,s^{-1}}$ independent of season (Fig. 5b). The friction velocity equivalent was $u_{*,top} \geq$ 0.35 m s^{-1} (not shown here). We here select this threshold as the transition from the decoupled sub-canopy layer (Ds) to the fully coupled canopy regime (C). For daytime conditions, we assume that above-canopy turbulent mixing is not limiting as long as sub-canopy mixing is sufficiently strong.

Comparing the probability of occurrence across all exchange regimes, one finds that the decoupled sub-canopy is the most abundant regime occupying approximately 65 and 88 % of the observations during the day and night, respectively, while the fully coupled canopy occurred 34 and 11 % and the decoupled ground layer $< 1\,\%$ of the time, respectively (Table 1).

4.4. Comparison of chamber-based soil and sub-canopy respiration

Figure 6 placed here.

Since the respiration components captured by the sub-canopy respiration Re_{sub} and the soil respiration chambers Re_{soil} are largely identical, one can investigate the differences between these fluxes with regard to turbulent mixing strength relevant for the computation of NEE. Both quantities include contributions by the roots, litter, and microbes as well as fine woody detritus, while Re_{soil} additionally captures the respiration from coarse woody debris and the understory vegetation. The fraction of the latter two components to total ecosystem respiration, however, is typically small, particularly at our site, which is characterized by low light levels and few coarse woody debris on the ground.

For the decoupled sub-canopy regime (Ds), Re_{sub} was sensitive to the turbu-

lent mixing strength, while Re_{soil} was independent of $\sigma_{w,sub}$ (Fig. 6). Transitioning to a fully coupled canopy (C), Re_{sub} also became independent and approached values that were approximately 10 to 20 % lower compared to Re_{soil} for a given temperature class. Note that the boundaries of the temperature classes are equivalent since they were determined by fitting a quadratic regression of air versus soil temperature. The sub-canopy respiration observed for the highest temperatures was an exception since it failed to converge to a value independent of σ_w. Separating fluxes in this broad temperature class yielded that the sustained increase was caused by a small group of extreme values observed for very high temperatures $T > 26$ °C. Differences between the flow conditions in the sampling volume of each technique can explain the differences for the Ds regime: diffusion of CO_2 molecules out of the soil and transport through the sampling path of the sub-canopy EC system is limited by the weak turbulent mixing for $\sigma_{w,sub} \leq 0.10$ m s^{-1}. The sub-canopy transport in the dense canopy therefore remains limiting to the flux, despite the steepness of the vertical CO_2 gradient of several hundred ppm m^{-1}. In contrast, the transport inside the soil respiration chamber is different since both molecular diffusion and turbulent mixing are artificially enhanced by actively pumping air. CO_2 concentration gradients at the soil-air interface are similar for both technqiues. We emphasize that both respiration estimates Re_{sub} and Re_{soil} are biologically meaningful, while they show systematic differences arising from the mixing strength in their sampling volumes.

4.5. Improved carbon balance

Figure 7 placed here. Table 2 placed here.

We now proceed and compute the improved carbon balance using the pro-

posed framework with the exchange regimes and equations summarized in Table 1. Accounting for the advective losses to total ecosystem respiration for the decoupled sub-canopy regime (Ds) led to a close agreement between nighttime NEE $\equiv$ RE and the independently computed alternative ecosystem respiration RE_{alt} over a wide temperature range (Fig. 7). The interquartile range of RE_{alt} closely matched that of NEE for a given temperature bin, while the scatter in NEE was significantly larger. One must recall that stem and foliage respiration, which on average contributed 18 % and 22 % respectively to RE_{alt}, were modeled using air temperature as the only predictor (see Section 3.3). Hence, their estimates are expected to closely follow the temperature sensitivity of the model acting to reducing the scatter in RE_{alt}. In addition, the soil CO_2 efflux, which on average contributed the remaining 60 % to RE_{alt}, represent a spatial averages across six different chambers also acting to reduce the scatter. In contrast, the nighttime respiration computed as ($FCO_{2,top}$ + ΔS) derived using a 'traditional' filtering and gap-filling approach was significantly smaller by 36 % compared to both improved RE from the new framework and RE_{alt}. The traditional approach was based solely on single-level above-canopy EC fluxes with nighttime values filtered by a friction velocity criterion of $u_* \geq 0.35$ m s^{-1} determined from plotting ($FCO_{2,top}$ + ΔS) against u_* for several temperature bins (Goulden et al., 1996). Systematic discrepancies between RE and RE_{alt} were found only for the highest temperatures $T_{sub} \geq 23$ $^{\circ}C$ occurring during late summer. During this season, the trees increasingly experience soil moisture limitations in the late afternoon hours (Fig. 7), which leads to a reduction of photosynthesis and autotrophic respiration, and thus ecosystem respiration captured

by the EC fluxes. The soil moisture limitations may further dampen heterotrophic soil respiration, which enhances this effect. In contrast, stem and foliage respiration were modeled using a temperature-dependent model that lacks moisture limitations, while Re_{soil} showed a reduction during the dry, late summer (not shown here). These discrepancies however, had a negligible effect on the uncertainty of the carbon balance estimates since very few observations fell into the high temperature classes (see grey solid line in Fig. 7).

The annual improved NEE was significantly reduced compared to that derived from the 'traditional approach' yielding on average 622 gC m^{-2} yr^{-1} less carbon uptake (Tab. 2). The 6-year average of improved NEE was -479 gC m^{-2} yr^{-1} compared to -1101 gC m^{-2} yr^{-1} from the traditional approach. The difference between the two methods was attributed to an enhanced ecosystem respiration, while gross ecosystem productivity, computed as the residual from GEP=NEE-RE, remained almost unchanged. The GEP estimates agreed well with those predicted by Waring et al. (2008) for the same site using the process-based forest growth model 3-PG driven by observed meteorologic data. As expected, improving NEE was primarily accomplished by increasing nighttime NEE by including the advective losses estimated through the sub-canopy respiration (Eq. 3). The improved annual NEE agreed well estimates for a Douglas-Fir forest of similar age, stocking and climate (Chen et al., 2009; Jassal et al., 2010, 2007; Krishnan et al., 2009), and fit more favorably into global meta-analyses given the mean temperature and precipitation at the site (Luyssaert et al., 2007). Note that we did not apply an 'ecological plausibility filtering' to force RE>0 and GEP<0 μmol

m^{-2} s^{-1}. However, the fractions for these 'ecologically implausible' periods were 0.7 % and 2 % over the entire observational period, respectively. The positive GEP values were mainly associated with hours shortly after dawn and before dusk and may thus be biologically plausible, while the negative nighttime RE values are expected to result from random variability associated with turbulent fluxes. Given their small abundance, these anomalies have a negligible impact on annual NEE estimates. The fraction of observed nighttime NEE data retained to constrain the Arrhenius-type model used for gap-filling and to model daytime respiration was doubled compared to the traditional approach (35 % versus 17 %, respectively, Tab. 2). In contrast, the fractions of observed NEE during the day remained unchanged.

4.6. Limitations and risks of the approach

The improved NEE approach bears the risk of double-counting an unknown fraction of CO_2 molecules by adding the missing, advected sub-canopy respiration to NEE for the decoupled sub-canopy regime (Ds). In other words, our assumption of a 'hermetical' decoupling between the sub-canopy and above-canopy layers may not be correct in all instances. However, several observations support our claim that the diagnosed decoupling is meaningful and that a significant fraction of total ecosystem respiration is not captured by ($FCO_{2,top}$ + ΔS):

- The identified thresholds of $\sigma_{w,top} \geq 0.45\,\mathrm{m\,s^{-1}}$ and $\sigma_{w,sub} \geq 0.10\,\mathrm{m\,s^{-1}}$ for transition from the Ds to C regime agree well with the transition from the asymptotic to the linear response regime in the mixing strength (see Fig. 3c, and Section 4.1). This agreement suggests a cohesion between the physical transport and the biological signal of CO_2

sinks and sources in the canopy. A recent review of canopy flows in mountainous terrain by Belcher et al. (2008) also supports the assumption of decoupled canopy and sub-canopy layers from the flow aloft. Their explanation is based on fundamental differences in momentum and heat transport from the air to the canopy elements, in spite of significant above-canopy flows.

- For $\sigma_{w,top} \leq 0.45$ m s^{-1}, the traditional nighttime ($FCO_{2,top}$ + ΔS) indicated a dependence on turbulence mixing strength as well as on temperature (Fig. 5b). Since nighttime ecosystem respiration is primarily driven by temperature except for the late summer season where soil moisture may become limiting, this observation is evidence that the above-canopy EC flux does not integrate over all sinks and sources supporting the argument of Goulden et al. (1996). This underestimation is systematic for low turbulence conditions that are intrinsically related to the dense, tall overstory of the Douglas-fir trees and exacerbated by the sheltering topography.

- The variability of the sub-canopy flow and temperature fields and the resultant horizontal advection of sensible heat at the site was investigated by Thomas (2011). Both the vector and scalar field showed systematic variability that was dependent upon the time scale, the location within the domain, and the total size of the domain. Furthermore, horizontal advection of heat was significant and systematic in sign and magnitude for horizontal scales exceeding 180 m. We therefore consider our assumption of a systematic loss in ecosystem respiration through

advection to be plausible. However, the lack of direct evidence for the scalar similarity between the advective transport of carbon dioxide and sensible heat, and the absence of direct estimates of sub-canopy CO_2 advection such as in Staebler and Fitzjarrald (2004) remains a weakness of the investigation presented here.

In the literature, there exists indirect observational and modeling evidence for the importance of advection to the carbon dioxide budget: Sun et al. (2006) used a large eddy simulation method to model the transport of carbon dioxide for a similar tall forest in sloped mountainous terrain. They found that advection caused by drainage flows and a weak land breeze was a significant term in the scalar budget, which resulted in an underestimation of nighttime respiration of about 20 %. Despite the similarities in canopy architecture and geometry of the terrain between their study area and our site, their nighttime NEE was dominated by the vertical turbulent flux, which disagrees with our findings. However, their transport was dominated by the portion contributed by the sub-grid scale parameterizations, so a direct comparison cannot be done. Van Gorsel et al. (2007) and a follow-up study by van Gorsel et al. (2009) found indirect evidence for advective loss of carbon dioxide due to drainage flows. The authors investigated the temporal dynamics of (FCO_2 + ΔS) over the diurnal period showing a clear maximum during the early evening, whose magnitude agreed well with independent ecosystem respiration estimates from chambers. With progression of the night, the difference between the two respiration estimates increased indicating the growing importance of advective transport and loss of CO_2 in the simplified

carbon budget.

One must keep in mind that the transitions between all three exchange regimes are rather gradual, in spite of our definition of numerically exact thresholds. The significant variability in relationships between correlation coefficients, ecosystem carbon and water vapor fluxes, and turbulent mixing proxies will inevitably lead to a false classification of exchange regimes for individual periods. However, we expect the determined thresholds to be suitable for the purpose of constructing seasonal and annual carbon budgets. Errors resulting from miss-classification are assumed to be random and thus to cancel out over a sufficiently large sample size.

Double-counting of CO_2 molecules and the uncertainty associated with the determination of thresholds for the exchange regimes remain to be realistic limitations to the improved NEE approach. Its estimates may therefore serve as a lower limit for the strength of the terrestrial carbon sink resulting from a possibly overestimated ecosystem respiration. Considering that the well-documented nighttime limitation to the traditional EC approach results in a systematic underestimation of ecosystem respiration and an overestimation of the carbon sink, the framework proposed here may make an important contribution to the discussion of uncertainty in NEE estimates for tall, dense forests.

5. Conclusions

We arrive at the following conclusions with respect to our objectives listed in the introduction:

- The standard deviation of the vertical velocity variance σ_w was the

most suitable proxy for the turbulent mixing strength in this dense canopy. It is preferable over alternatives including the friction velocity since it is a direct measure of the turbulent kinetic energy rather than its momentum flux. It was more sensitive to alternative mechanisms generating turbulence creating additional mixing. Alternative mechanisms include wind directional shear in combination with significant above-canopy flows and strong stability, as well as sub-meso structures present in the sub-canopy (Thomas, 2011). The standard deviation of the vertical velocity variance is routinely calculated, which makes it readily available to the user.

- The proposed framework of exchange regimes was found to be meaningful with respect to both biological scalar signals and the physical transport of the turbulent eddies. In this dense canopy, it is imperative to have direct measurements of the sub-canopy mixing strength to estimate the vertical coupling. We therefore recommend including continuous, concurrent sub-canopy EC observations to the standard measurement protocol in addition to the traditional above-canopy flux measurements in dense, tall forests.

- The improved NEE method led to a significant enhancement of the fraction of observations used to parametrize the analytical gap-filling models and to compute the annual carbon budget. For nighttime data, this fraction was doubled compared to the traditional approach based on above-canopy EC fluxes at a single level filtered by a u_* criterion. It may therefore help to add more dense forests to continental and

global scale carbon cycle studies by correcting the bias toward sites with shorter and more open canopies characterized by stronger flows and more vigorous turbulent mixing.

- The annual NEE computed from the improved method was significantly lower than that of the traditional approach by ≈ 620 gC m^{-2} yr^{-1}. The improved estimated strength of the carbon sink for this forest compared better to estimates reported for similar ecosystems. Based on the discussion of risks and limitations of the method, this estimate can be regarded as a lower limit.

- Improving upon the traditional approach used to compute NEE from single-level EC observations was not difficult. The improved method does not require additional instrumentation or measurements assuming that EC observations from at least two levels exist. It can readily be applied to historic data. The thresholds for the transitions between exchange regimes are expected to be site-specific, while their underlying concepts and correlations can be transferred. Since NEE estimates from the improved and traditional approaches yielded large discrepancies, we conclude that dense and tall forests do not lend themselves to standardized processing, which has been proposed for various continental networks. The benefit of having an additional, lower boundary for NEE reflecting an enhanced ecosystem respiration may, however, outweigh the additional effort required to determine the exchange regimes and to compute sub-canopy respiration.

6. Acknowledgements

This research was supported by the U.S. Department of Energy (DOE), Office of Science (BER), contract DE-FG02-06ER64318, and the National Science Foundation, Physical & Dynamic Meteorology, award AGS 0955444.

References

Acevedo, O. C., Moraes, O. L. L., Degrazia, G. A., Fitzjarrald, D. R., Manzi, A. O., Campos, J. G., 2009. Is friction velocity the most appropriate scale for correcting nocturnal carbon dioxide fluxes? Agric. For. Meteorol. 149 (1), 1–10.

Atkin, O. K., Tjoelker, M. G., 2003. Thermal acclimation and the dynamic response of plant respiration to temperature. Trends in Plant Science 8 (7), 343–351.

Aubinet, M., Berbigier, P., Bernhofer, C. H., Cescatti, A., Feigenwinter, C., Granier, A., Grunwald, T. H., Havrankova, K., Heinesch, B., Longdoz, B., Marcolla, B., Montagnani, L., Sedlak, P., 2005. Comparing CO_2 storage and advection conditions at night at different carboeuroflux sites. Boundary-Layer Meteorol. 116 (1), 63–94.

Aubinet, M., Feigenwinter, C., Heinesch, B., Bernhofer, C., Canepa, E., Lindroth, A., Montagnani, L., Rebmann, C., Sedlak, P., van Gorsel, E., 2010. Direct advection measurements do not help to solve the night-time CO_2 closure problem: Evidence from three different forests. Agric. For. Meteorol. 150 (5), 655–664.

858 Aubinet, M., Grelle, A., Ibrom, A., Rannik, U., Moncrieff, J., Foken, T.,
859 Kowalski, A. S., Martin, P. H., Berbigier, P., Bernhofer, C., Clement, R.,
860 Elbers, J., Granier, A., Grunwald, T., Morgenstern, K., Pilegaard, K.,
861 Rebmann, C., Snijders, W., Valentini, R., Vesala, T., 2000. Estimates
862 of the annual net carbon and water exchange of forests: The euroflux
863 methodology. Advances in Ecological Research, 30, 113–175.

864 Baldocchi, D. D., 2003. Assessing the eddy covariance technique for evaluat-
865 ing carbon dioxide exchange rates of ecosystems: past, present and future.
866 Global Change Biol. 9 (4), 479–492.

867 Belcher, S. E., Finnigan, J. J., Harman, I. N., 2008. Flows through forest
868 canopies in complex terrain. Ecologic. Appl. 18 (6), 1436–1453.

869 Burns, S. P., Sun, J., Lenschow, D. H., Oncley, S. P., Stephens, B. B., Yi,
870 C., Anderson, D. E., Hu, J., Monson, R. K., 2011. Atmospheric stability
871 effects on wind fields and scalar mixing within and just above a subalpine
872 forest in sloping terrain. Boundary-Layer Meteorol. 138 (2), 231–262.

873 Chen, B., Black, T. A., Coops, N. C., Krishnan, P., Jassal, R., Bruemmer,
874 C., Nesic, Z., 2009. Seasonal controls on interannual variability in carbon
875 dioxide exchange of a near-end-of rotation douglas-fir stand in the pacific
876 northwest, 1997-2006. Global Change Biol. 15 (8), 1962–1981.

877 Dupont, S., Irvine, M. R., Bonnefond, J.-M., Lamaud, E., Brunet, Y., 2012.
878 Turbulent structures in a pine forest with a deep and sparse trunk space:
879 Stand and edge regions. Boundary-Layer Meteorol. 143 (2), 309–336.

880 Falk, M., Wharton, S., Schroeder, M., Ustin, S., Paw U, K. T. P., 2008. Flux
881 partitioning in an old-growth forest: seasonal and interannual dynamics.
882 Tree Physiol. 28 (4), 509–520.

883 Feigenwinter, C., Bernhofer, C., Vogt, R., 2004. The influence of advection on
884 the short term CO_2-budget in and above a forest canopy. Boundary-Layer
885 Meteorol. 113 (2), 201–224.

886 Foken, T., Meixner, F. X., Falge, E., Zetzsch, C., Serafimovich, A., Barg-
887 sten, A., Behrendt, T., Biermann, T., Breuninger, C., Dix, S., Gerken,
888 T., Hunner, M., Lehmann-Pape, L., Hens, K., Jocher, G., Kesselmeier, J.,
889 Lueers, J., Mayer, J. C., Moravek, A., Plake, D., Riederer, M., Ruetz, F.,
890 Scheibe, M., Siebicke, L., Soergel, M., Staudt, K., Trebs, I., Tsokankunku,
891 A., Welling, M., Wolff, V., Zhu, Z., 2012. Coupling processes and exchange
892 of energy and reactive and non-reactive trace gases at a forest site - results
893 of the eger experiment. Atmos. Chem. Phys. 12 (4), 1923–1950.

894 Foken, T., Wichura, B., 1996. Tools for quality assessment of surface-based
895 flux measurements. Agric. For. Meteorol. 78, 83–105.

896 Gockede, M., Michalak, A. M., Vickers, D., Turner, D. P., Law, B. E., 2010.
897 Atmospheric inverse modeling to constrain regional-scale CO_2 budgets at
898 high spatial and temporal resolution. J. Geophys. Res.-Atmos. 115.

899 Goulden, M. L., Munger, J. W., Fan, S. M., Daube, B. C., Wofsy, S. C.,
900 1996. Measurements of carbon sequestration by long-term eddy covariance:
901 Methods and a critical evaluation of accuracy. Global Change Biol. 2 (3),
902 169–182.

Irvine, J., Law, B. E., 2002. Contrasting soil respiration in young and old-growth ponderosa pine forests. Global Change Biol. 8 (12), 1183–1194.

Jassal, R. S., Black, T. A., Cai, T., Ethier, G., Pepin, S., Bruemmer, C., Nesic, Z., Spittlehouse, D. L., Trofymow, J. A., 2010. Impact of nitrogen fertilization on carbon and water balances in a chronosequence of three douglas-fir stands in the pacific northwest. Agric. For. Meteorol. 150 (2), 208–218.

Jassal, R. S., Black, T. A., Cai, T. B., Morgenstern, K., Li, Z., Gaumont-Guay, D., Nesic, Z., 2007. Components of ecosystem respiration and an estimate of net primary productivity of an intermediate-aged douglas-fir stand. Agric. For. Meteorol. 144 (1-2), 44–57.

Krishnan, P., Black, T. A., Jassal, R. S., Chen, B., Nesic, Z., 2009. Inter-annual variability of the carbon balance of three different-aged douglas-fir stands in the pacific northwest. J. Geophys. Res.-Biogeosci. 114.

Law, B. E., Baldocchi, D. D., Anthoni, P. M., 1999. Below-canopy and soil CO_2 fluxes in a ponderosa pine forest. Agric. For. Meteorol. 94 (3-4), 171–188.

Luyssaert, S., Janssens, I. A., Sulkava, M., Papale, D., Dolman, A. J., Reichstein, M., Hollmen, J., Martin, J. G., Suni, T., Vesala, T., Loustau, D., Law, B. E., Moors, E. J., 2007. Photosynthesis drives anomalies in net carbon-exchange of pine forests at different latitudes. Global Change Biol. 13 (10), 2110–2127.

925 Mahrt, L., Thomas, C., Prueger, J., 2009. Space-time structure of mesoscale
926 modes in the stable boundary layer. Quart. J. Roy. Meteorol. Soc. 135,
927 67–75.

928 Mahrt, L., Thomas, C., Richardson, S., Seaman, N., Stauffer, D., Zeeman,
929 M. J., 2012. Generation of weak mixing for very stable and weak-wind
930 conditions. Boundary-Layer Meteorol., DOI: 10.1007/s10546–012–9782–x.

931 Martin, J. G., Phillips, C. L., Schmidt, A., Irvine, J., Law, B. E., 2012.
932 High-frequency analysis of the complex linkage between soil CO_2 fluxes,
933 photosynthesis and environmental variables. Tree Physiol. 32 (1), 49–64.

934 Matson, P., Johnson, L., Billow, C., Miller, J., Pu, R. L., 1994. Seasonal
935 patterns and remote spectral estimation of canopy chemistry across the
936 oregon transect. Ecologic. Appl. 4 (2), 280–298.

937 Misson, L., Baldocchi, D. D., Black, T. A., Blanken, P. D., Brunet, Y.,
938 Yuste, J. C., Dorsey, J. R., Falk, M., Granier, A., Irvine, M. R., Jarosz, N.,
939 Lamaud, E., Launiainen, S., Law, B. E., Longdoz, B., Loustau, D., McKay,
940 M., Paw, K. T., Vesala, T., Vickers, D., Wilson, K. B., Goldstein, A. H.,
941 2007. Partitioning forest carbon fluxes with overstory and understory eddy-
942 covariance measurements: A synthesis based on fluxnet data. Agric. For.
943 Meteorol. 144 (1-2), 14–31.

944 Papale, D., Reichstein, M., Aubinet, M., Canfora, E., Bernhofer, C., Kutsch,
945 W., Longdoz, B., Rambal, S., Valentini, R., Vesala, T., Yakir, D., 2006.
946 Towards a standardized processing of net ecosystem exchange measured

with eddy covariance technique: algorithms and uncertainty estimation. Biogeosci. 3 (4), 571–583.

Paw U, K. T., Brunet, Y., Collineau, S., Shaw, R. H., Maitani, T., Qiu, J., Hipps, L., 1992. Evidence of turbulent coherent structures in and above agricultural plant canopies. Agric. For. Meteorol. 61, 55–68.

Raupach, M. R., Finnigan, J. J., Brunet, Y., 1996. Coherent eddies and turbulence in vegetation canopies: the mixing-layer analogy. Boundary-Layer Meteorol. 78, 351–382.

Reich, P. B., Tjoelker, M. G., Pregitzer, K. S., Wright, I. J., Oleksyn, J., Machado, J.-L., 2008. Scaling of respiration to nitrogen in leaves, stems and roots of higher land plants. Ecology Letters 11 (8), 793–801.

Ruppert, J., Mauder, M., Thomas, C., Lueers, J., 2006. Innovative gap-filling strategy for annual sums of CO_2 net ecosystem exchange. Agric. For. Meteorol. 138, 5–18.

Scanlon, T. M., Albertson, J. D., 2001. Turbulent transport of carbon dioxide and water vapor within a vegetation canopy during unstable conditions: Identification of episodes using wavelet analysis. J. Geophys. Res. Atmos. 106 (D7), 7251–7262.

Serafimovich, A., Thomas, C., Foken, T., 2011. Vertical and horizontal transport of energy and matter by coherent motions in a tall spruce canopy. Boundary-Layer Meteorol. 140, 429–451.

Shaw, R. H., Zhang, X. J., 1992. Evidence of pressure-forced turbulent-flow in a forest. Boundary-Layer Meteorol. 58 (3), 273–288.

970 Staebler, R. M., Fitzjarrald, D. R., 2004. Observing subcanopy CO_2 advec-
971 tion. Agric. For. Meteorol. 122 (3-4), 139–156.

972 Stephens, B. B., Watt, A., Maclean, G. D., 2006. An autonomous inexpensive
973 robust CO_2 analyzer (aircoa). In: 13th WMO/IAEA Meeting of Experts
974 on Carbon Dioxide Concentration and Related Tracers Measurement Tech-
975 niques. Boulder, CO, USA.

976 Stull, R. B., 2000. Meteorology for scientists and engineers, 2nd Edition.
977 Gary Garlson, Brooks/Cole, 502 pp.

978 Sun, H. Z., Clark, T. L., Stull, R. B., Black, T. A., 2006. Two-dimensional
979 simulation of airflow and carbon dioxide transport over a forested mountain
980 - part ii. carbon dioxide budget analysis and advection effects. Agric. For.
981 Meteorol. 140 (1-4), 352–364.

982 Suyker, A. E., Verma, S. B., Burba, G. G., 2003. Interannual variability in
983 net CO_2 exchange of a native tallgrass prairie. Global Change Biol. 9 (2),
984 255–265.

985 Thomas, C., 2011. Variability of subcanopy flow, temperature, and horizontal
986 advection in moderately complex terrain. Boundary-Layer Meteorol. 139,
987 61–81.

988 Thomas, C., Foken, T., 2002. Re-evaluation of integral turbulence charac-
989 teristics and their parameterisations. In: 15th Symposium on Boundary
990 Layers and Turbulence. Am.Meteorol.Soc., Wageningen, The Netherlands,
991 pp. 129–132.

992 Thomas, C., Foken, T., 2007. Flux contribution of coherent structures and its
993 implications for the exchange of energy and matter in a tall spruce canopy.
994 Boundary-Layer Meteorol. 123, 317–337.

995 Thomas, C., Law, B., Irvine, J., Martin, J., Pettijohn, J., Davis, K., 2009.
996 Seasonal hydrology explains inter-annual and seasonal variation in carbon
997 and water exchange in a semi-arid mature ponderosa pine forest in central
998 oregon. J. Geophys. Res.-Biogeosci. 114, G04006.

999 Thomas, C., Martin, J. G., Goeckede, M., Siqueira, M. B., Foken, T., Law,
1000 B. E., Loescher, H. W., Katul, G., 2008. Estimating daytime subcanopy
1001 respiration from conditional sampling methods applied to multi-scalar high
1002 frequency turbulence time series. Agric. For. Meteorol. 148 (8-9), 1210–
1003 1229.

1004 Tjoelker, M. G., Oleksyn, J., Reich, P. B., 2001. Modelling respiration of
1005 vegetation: evidence for a general temperature-dependent q(10). Global
1006 Change Biol. 7 (2), 223–230.

1007 van Gorsel, E., Delpierre, N., Leuning, R., Black, A., Munger, J. W., Wofsy,
1008 S., Aubinet, M., Feigenwinter, C., Beringer, J., Bonal, D., Chen, B., Chen,
1009 J., Clement, R., Davis, K. J., Desai, A. R., Dragoni, D., Etzold, S., Gruen-
1010 wald, T., Gu, L., Heinesch, B., Hutyra, L. R., Jans, W. W. P., Kutsch, W.,
1011 Law, B. E., Leclerc, M. Y., Mammarella, I., Montagnani, L., Noormets,
1012 A., Rebmann, C., Wharton, S., 2009. Estimating nocturnal ecosystem res-
1013 piration from the vertical turbulent flux and change in storage of CO_2.
1014 Agric. For. Meteorol. 149 (11), 1919–1930.

1015 Van Gorsel, E., Leuning, R., Cleugh, H. A., Keith, H., Suni, T., 2007. Noctur-
1016 nal carbon efflux: reconciliation of eddy covariance and chamber measure-
1017 ments using an alternative to the u*-threshold filtering technique. Tellus
1018 B 59 (3), 397–403.

1019 Vickers, D., Thomas, C., Pettijohn, C., Martin, J. G., Law, B., 2012. Five
1020 years of carbon fluxes and inherent water-use efficiency at two semi-arid
1021 pine forests with different disturbance histories. Tellus B 64, 17159.

1022 Waring, R., Nordmeyer, A., Whitehead, D., Hunt, J., Newton, M., Thomas,
1023 C., Irvine, J., 2008. Why productivity of douglas-fir is higher in new
1024 zealand than in its native range. Forest Ecology & Management 255, 4040–
1025 4046.

1026 Webb, E. K., Pearman, G. I., Leuning, R., 1980. Correction of the flux
1027 measurements for density effects due to heat and water vapour transfer.
1028 Quart. J. Roy. Meteorol. Soc. 106, 85–100.

1029 Wharton, S., Schroeder, M., Paw U, K. T., Falk, M., Bible, K., 2009. Tur-
1030 bulence considerations for comparing ecosystem exchange over old-growth
1031 and clear-cut stands for limited fetch and complex canopy flow conditions.
1032 Agric. For. Meteorol. 149 (9), 1477–1490.

1033 Wilczak, J. M., Oncley, S. P., Stage, S. A., 2001. Sonic anemometer tilt
1034 correction algorithms. Boundary-Layer Meteorol. 99, 127–150.

1035 Zeeman, M. J., Eugster, W., Thomas, C., 2012. Concurrency of coher-
1036 ent structures and conditionally sampled daytime sub-canopy respiration.
1037 Boundary-Layer Meteorol., DOI 10.1007/s10546–012–9745–2.

Table 1: Mass balance equations for net ecosystem exchange (NEE) comprised of the vertical turbulent CO_2 flux (FCO_2), the temporal change in storage term (ΔS), net photosynthesis (GEP), and subcanopy respiration (Re_{sub}, determined following Thomas et al. (2008) applied to the sub-canopy EC observations, see Section 3.2) depending on observation height within the above-canopy layer (*top*) or sub-canopy layer (*sub*) for the three different exchange regimes described in Section 2: Decoupled ground layer (Dg), decoupled sub-canopy (Ds), and fully coupled canopy (C). Also shown are the determined thresholds of the standard deviation of the vertical velocity variance, $\sigma_w = \sqrt{\overline{w\prime w\prime}}$, where $w\prime$ is the vertical velocity perturbation.

Exchange regime	Mass balance		Criteria & Thresholds		Fraction[#]	
	Day	Night	Day	Night	Day	Night
Dg	NEE not measurable	NEE not measurable	$\sigma_{w,sub} < 0.3$ m s^{-1}	$\sigma_{w,sub} < 0.3$ m s^{-1}	< 1 %	< 1 %
Ds	NEE = $FCO_{2,top}$ + Re_{sub} + (GEP_{sub}) + ΔS	NEE = $FCO_{2,top}$ + Re_{sub} + ΔS	$0.03 \leq \sigma_{w,sub} < 0.10$ m s^{-1}	$0.03 \leq \sigma_{w,sub} < 0.10$ m s^{-1}	65 %	88 %
C	NEE = $FCO_{2,top}$ + ΔS	NEE = $FCO_{2,top}$ + ΔS	$\sigma_{w,sub} \geq 0.10$ m s^{-1}	$\sigma_{w,sub} \geq 0.10$ m s^{-1} & $\sigma_{w,top} \geq 0.45$ m s^{-1}	34 %	11 %

[#]: averaged over entire observational period 2006 through 2011

Table 2: Annual sums of carbon balance components for the observational period 2006 through 2011: improved net ecosystem exchange (NEE), ecosystem respiration (RE), and gross ecosystem productivity (GEP) computed using the equations listed in Table 1 from both above- and sub-canopy EC data. For comparison, estimates are also provided for a traditional approach to compute components solely based on the above-canopy EC observations with nighttime fluxes filtered by a critical threshold of $u_{*,top} \geq 0.35\,\mathrm{m\,s^{-1}}$ (NEE_{trad}, RE_{trad}, and GEP_{trad}). Statistics are provided for percentage (p) of observed (obs) and modeled (mod) data for day (d) and night (n) conditions. Also listed are the annual sums of alternative ecosystem respiration (RE_{alt}) based on scaled soil CO_2 efflux chambers (Re_{soil}), and modeled stem (Re_{st}) and foliage respiration (Re_{fol}) described in Section 3.3. Gaps in EC data were filled using Arrhenius type and Michaelis-Menthen type models fitted to the night- and daytime data, respectively, for each year (see Ruppert et al., 2006; Thomas et al., 2009, for details). NEE < 0 indicates a net carbon sink.

	Improved approach					Traditional approach					Difference=			
	Two heights; mixing based on σ_w					Single height; mixing based on u_*					Improved-Traditional			eco
				p (obs/mod$^+$)					p (obs/mod$^+$)					
Year	NEE	RE	GEP	d&n	n	NEE_{trad}	RE_{trad}	GEP_{trad}	d&n	n	Δ NEE	Δ RE	Δ GEP	RE_{alt}
	[gC m^{-2} yr^{-1}]			[%]		[gC m^{-2} yr^{-1}]			[%]		[gC m^{-2} yr^{-1}]			[gC m^{-2} y
2006*	-694	1972	-2666	37/63	31/69	-1348	1254	-2603	39/61	15/85	655	718	63	2086
2007	-563	2009	-2572	52/48	48/52	-1258	1233	-2492	48/52	20/80	695	776	-80	2076
2008	-495	2092	-2588	48/52	46/54	-1121	1557	-2678	49/51	21/79	626	535	91	1994
2009	-305	2291	-2596	40/60	40/60	-882	1689	-2571	41/59	18/81	577	602	-25	1976
2010	-336	2231	-2567	33/67	32/68	-926	1599	-2526	41/59	20/80	590	632	-42	1964
2011	-482	1847	-2329	16/84	15/85	-1072	1275	-2347	21/79	9/91	590	572	18	2008

*: annual sum was computed over period 01-May-2006 through 01-May-2007; model coefficients determined from observations in 2007 were used for gap-filling.

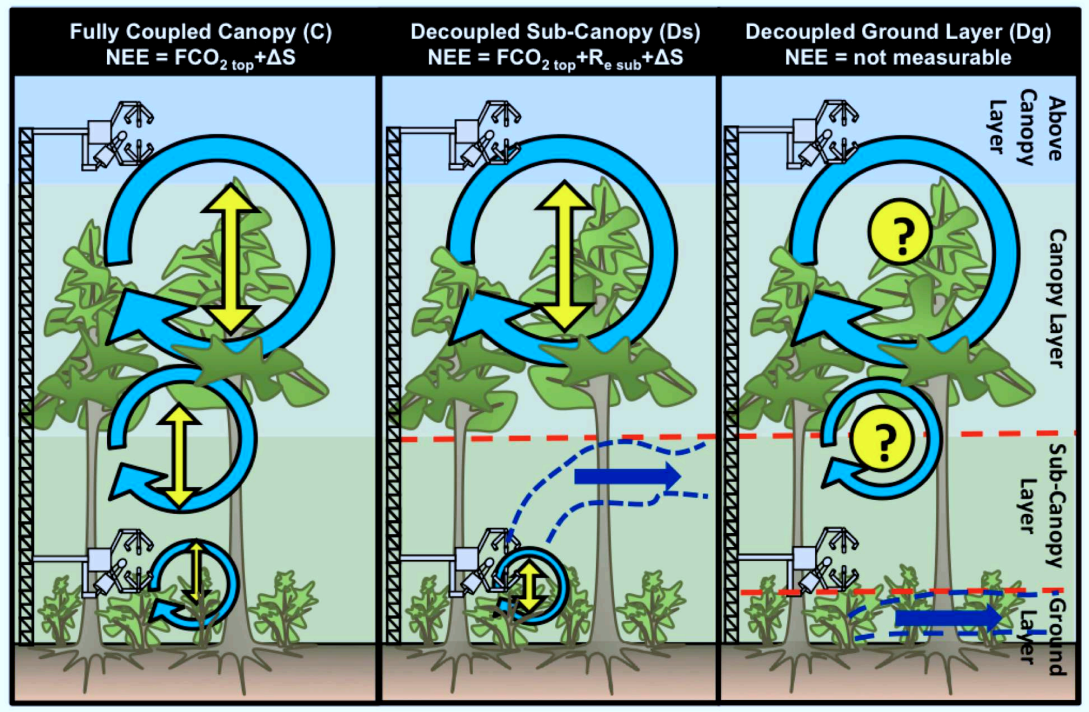

Figure 1: Illustration of the conceptual framework used to improve estimates of net ecosystem exchange (NEE) in tall, dense canopies. The vertical canopy coupling decreases from left to right from the fully coupled canopy (C), over the decoupled sub-canopy (Ds), to the decoupled ground layer (Dg) regimes. For the fully coupled canopy, it is assumed that the above-canopy eddy covariance (EC) flux ($FCO_{2,top}$) integrates the turbulent exchange of all carbon sinks and sources. For the decoupled sub-canopy regime, the above-canopy EC flux only integrates over sinks and sources located in the overstory, while the sub-canopy EC observations can be used to indirectly determine the advective loss through accounting for the sub-canopy respiration (Re_{sub}). For the decoupled ground layer regime, turbulent mixing is very weak and advection is assumed to be the dominant term in the carbon balance, which is not captured by any of the EC systems. ΔS is the temporal change of the storage term. Horizontal red dashed lines indicate decoupling between layers, dark blue arrows symbolize advection, and yellow vertical arrows turbulent exchange. Note that the light-blue circles symbolize turbulent structures in general, and not specific flow modes or length scales. See Section 2 for additional explanation.

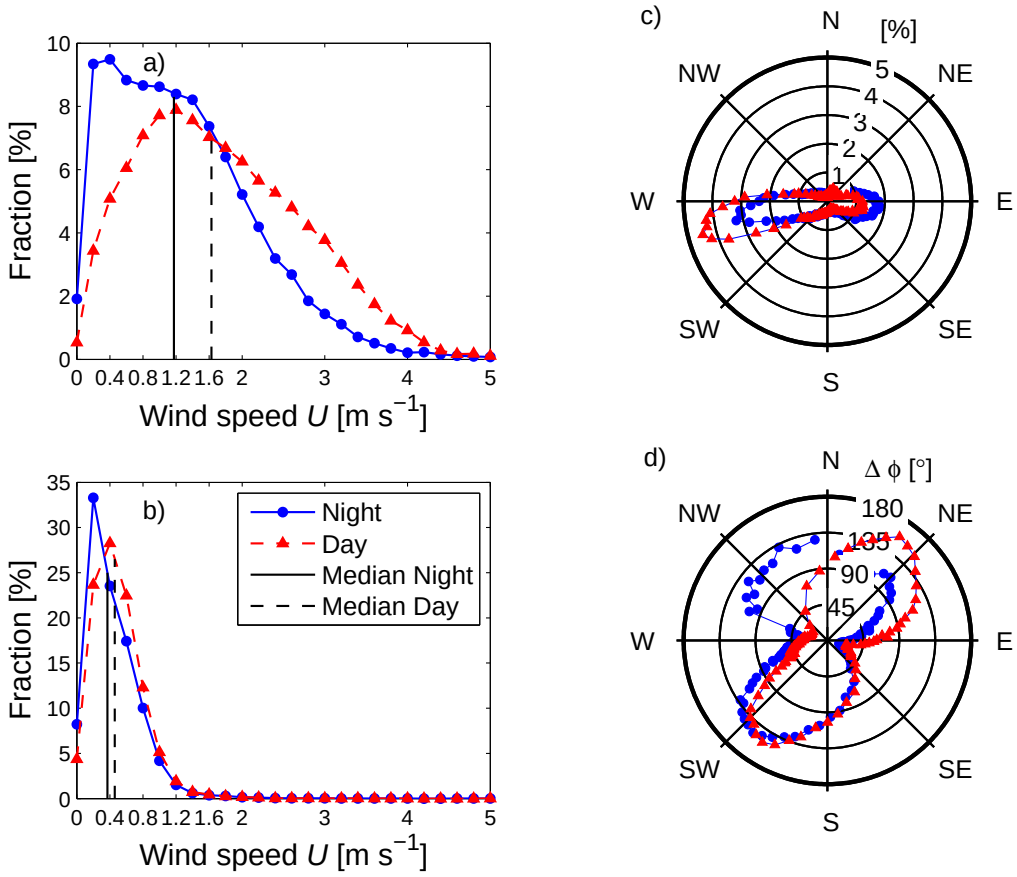

Figure 2: Characteristics of the mean flow at the dense, mature Douglas-Fir site observed between Mar 2006 and Nov 2011 as a function of the light regime: Probability density functions of the a) above-canopy (38.4 m agl) and b) sub-canopy (4 m agl) horizontal wind speeds, and c) above-canopy wind directions. Subplot d) shows the wind direction difference between above- and sub-canopy flow, $\Delta\phi$, i.e., the dimensional wind directional shear, as a function of the above-canopy wind direction.

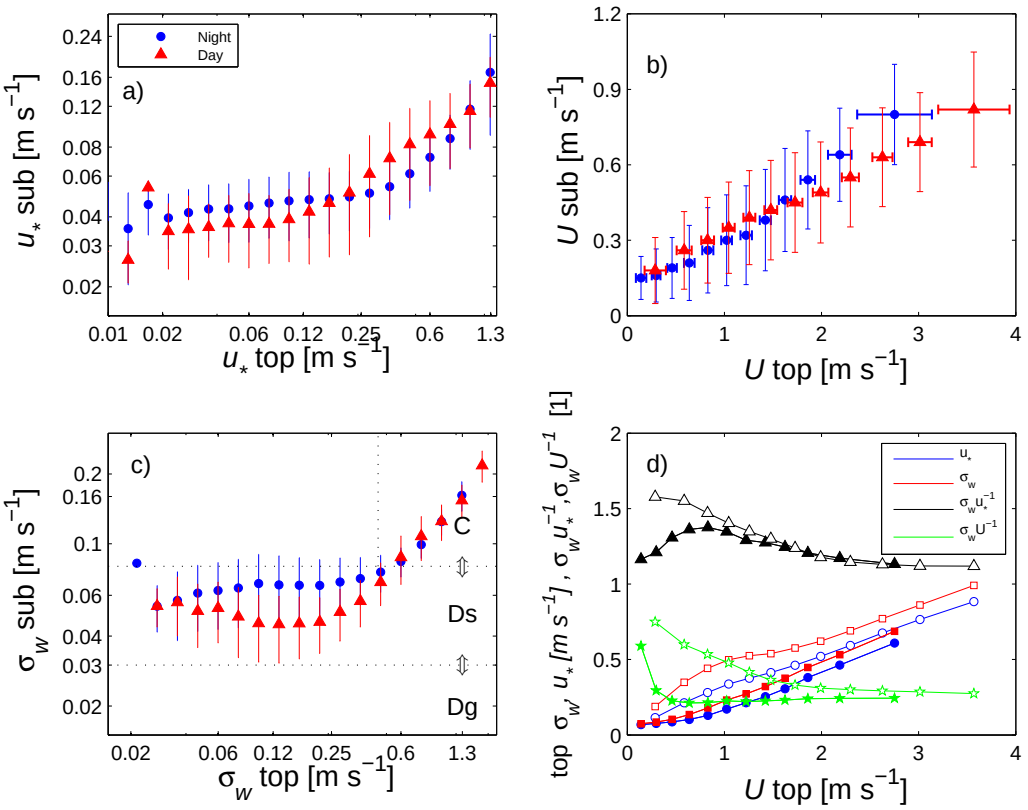

Figure 3: Comparison of various mixing indicators between the above-canopy (*top*) and sub-canopy (*sub*) levels: Friction velocity u_*, horizontal wind speed U, standard deviation of the vertical velocity variance σ_w, integral turbulence characteristic of the vertical velocity $\sigma_w u_*^{-1}$, and integral turbulence intensity $\sigma_w U^{-1}$. In subplot d), symbols are for u_* (circles), σ_w (squares), $\sigma_w u_*^{-1}$ (triangles), and $\sigma_w U^{-1}$ (pentagrams); filled symbols stand for night, and open symbols for day. Data were binned, bars represent one standard deviation of data within each bin. Subplot c) also contains the thresholds (dotted lines) used to define the three proposed exchange regimes: fully coupled canopy (C), decoupled sub-canopy (Ds), and decoupled ground layer (Dg), see Section 2 for details.

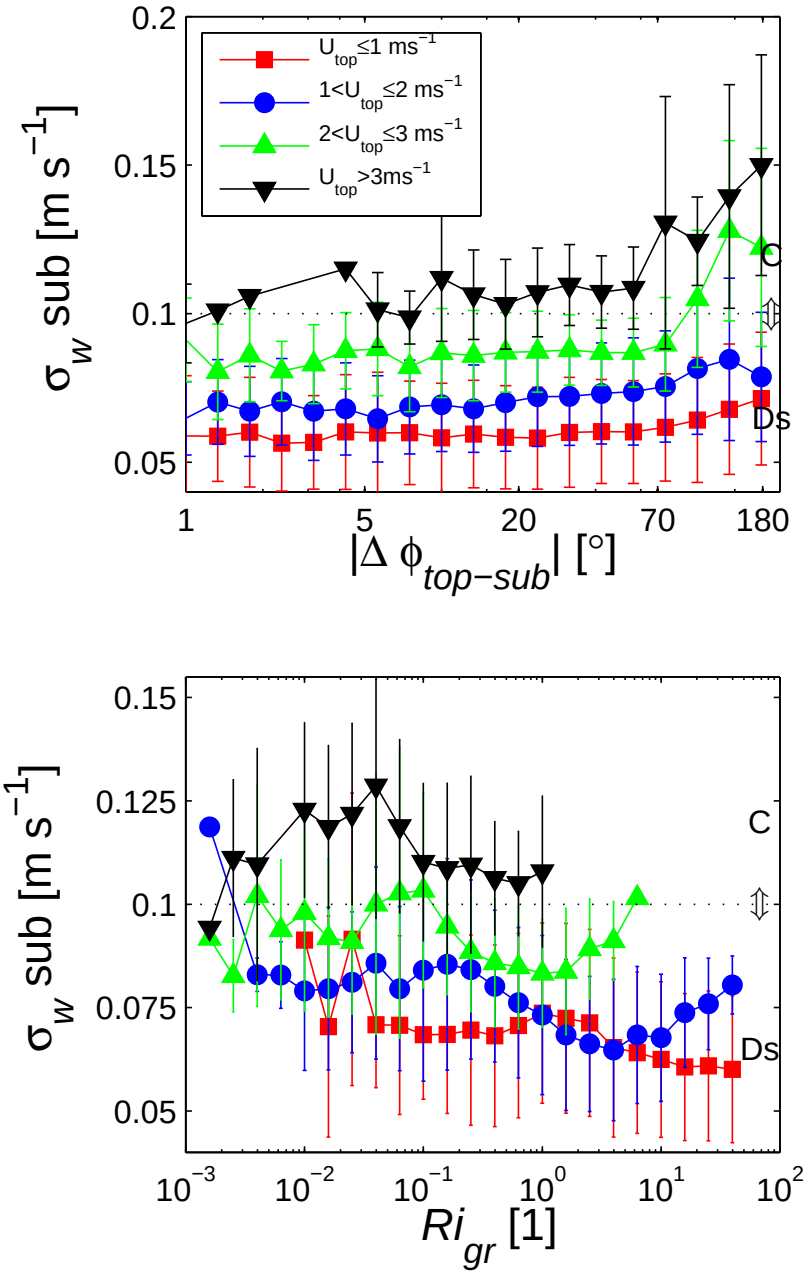

Figure 4: Enhancement of turbulent mixing through wind directional shear for different above-canopy horizontal wind speed classes (U_{top}) : a) standard deviation of the vertical velocity variance σ_w as a function of the wind direction difference between above- and sub-canopy flows $|\Delta\phi_{top-sub}|$, and b) σ_w as a function of the canopy gradient Richardson number Ri_{gr}. The threshold of $\sigma_{w,sub}$= 0.10 m s^{-1} used to delineate the exchange regimes decoupled sub-canopy (Ds) and fully coupled canopy (C) is also marked (dotted line).

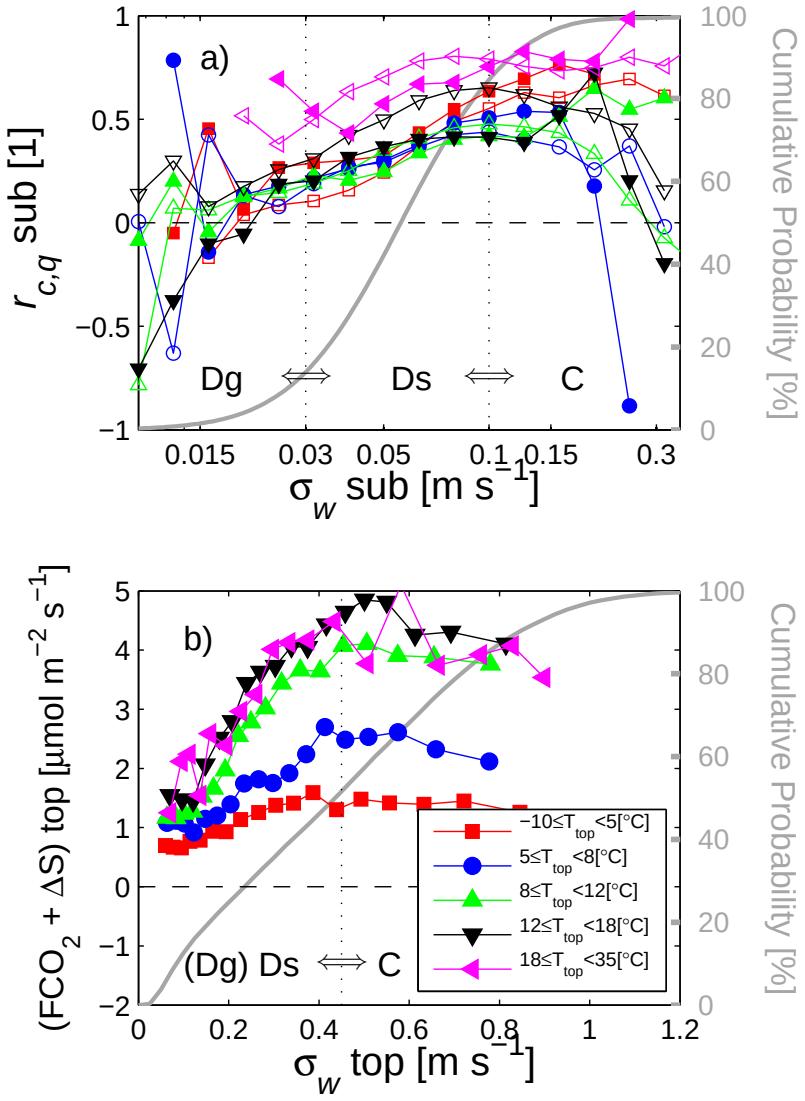

Figure 5: Determination of thresholds for the three exchange regimes: Fully coupled canopy (C), decoupled sub-canopy (Ds), decoupled ground layer (Dg); a) Correlation coefficient between perturbations of carbon dioxide and water vapor mixing ratios $r_{c,q}$ as a function of the turbulent mixing strength in the sub-canopy (sub) σ_w, and b) Nighttime net ecosystem exchange (NEE) as a function of the turbulent mixing strength above the canopy (top) σ_w for different air temperature classes (T_{top}). Each temperature class contains approximately 8000 30-min values. Also shown are the cumulative probability densities (grey lines) of σ_w combined for both night- and daytime data. Open symbols depict daytime, while closed symbols are for nighttime data. Error bars were omitted for clarity of presentation, but scatter was significant.

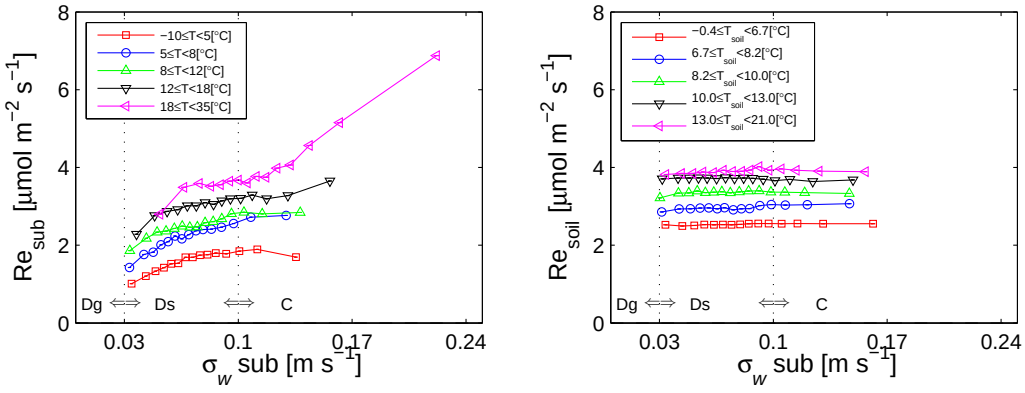

Figure 6: Comparing a) sub-canopy respiration Re_{sub} determined from the subcanopy EC data following Thomas et al. (2008), and b) chamber-based Soil CO_2 efflux Re_{soil} against the subcanopy turbulence mixing strength $\sigma_{w,sub}$ for classes of sub-canopy air T and soil temperature T_{soil} measured near the surface. Vertical dotted lines indicate the thresholds used to delineate the exchange regimes: fully coupled canopy (C), decoupled sub-canopy (Ds), and decoupled ground layer (Dg). Error bars were omitted for clarity of presentation, but scatter was significant.

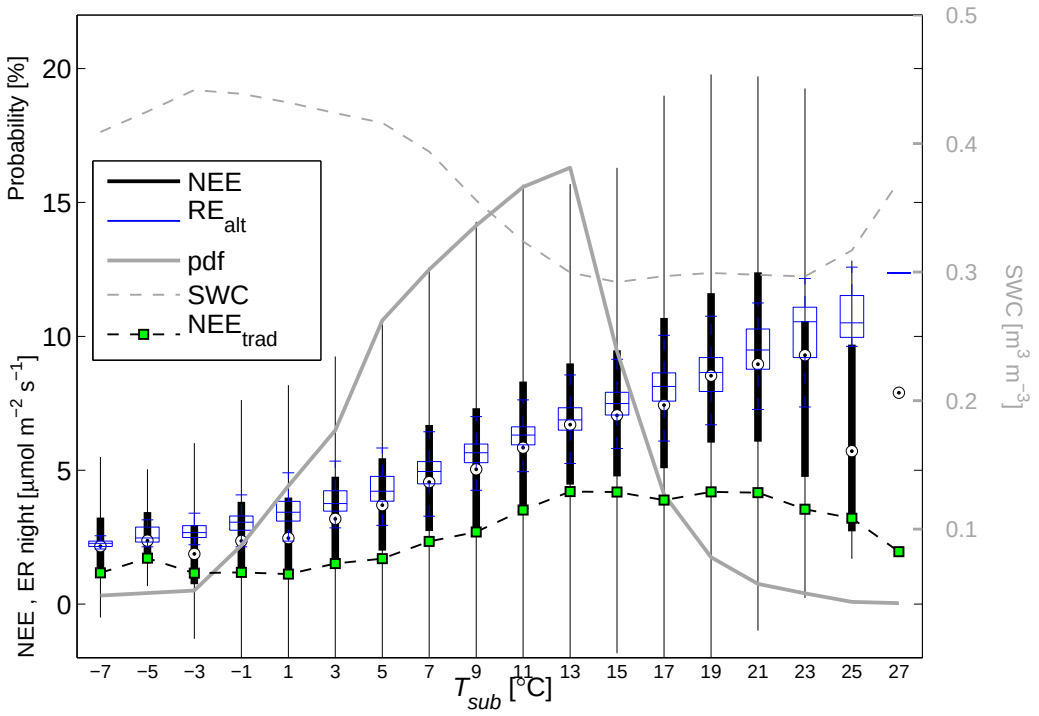

Figure 7: Temperature sensitivity of the improved estimates of nighttime net ecosystem exchange (NEE, for equations see Table 1), alternative ecosystem respiration (RE_{alt}) computed from scaled soil CO_2 efflux chambers and modeled stem and foliage respiration (see Section 3.3), and the 'traditional' single-level net ecosystem exchange using a critical u_* threshold (NEE_{trad}=$FCO_{2,top}$ + ΔS, see Section 4.5) for the observational period 2006 through 2011. NEE and RE_{alt} are presented in boxplots, in which the box is bounded by the 25 % and 75 % percentiles and the median is represented by a circle or horizontal line, respectively; length of the whiskers corresponds to 2.7σ or 99 % of the data in each bin. Also shown is the probability density function (pdf) of data across the sub-canopy air temperature bins T_{sub} of 2 K width, and the volumetric soil water content SWC (y-axis on the right).